Applied Physics Express

The Japan Society of Applied Physics

LETTER • OPEN ACCESS

Demonstration of low forward voltage InGaN-based red LEDs

To cite this article: Daisuke Iida *et al* 2020 *Appl. Phys. Express* **13** 031001

View the article online for updates and enhancements.

This content was downloaded from IP address 109.171.137.210 on 08/03/2020 at 09:43

OPEN ACCESS
Applied Physics Express 13, 031001 (2020)
https://doi.org/10.35848/1882-0786/ab7168

LETTER

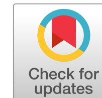

Demonstration of low forward voltage InGaN-based red LEDs

Daisuke Iida, Zhe Zhuang, Pavel Kirilenko, Martin Velazquez-Rizo, and Kazuhiro Ohkawa*

Computer, Electrical and Mathematical Sciences and Engineering (CEMSE) Division, King Abdullah University of Science and Technology (KAUST), Thuwal 23955-6900, Saudi Arabia

*E-mail: kazuhiro.ohkawa@kaust.edu.sa

Received December 23, 2019; revised January 27, 2020; accepted January 28, 2020; published online February 11, 2020

Here we report InGaN-based red light-emitting diodes (LEDs) grown on ($\bar{2}01$) β-Ga_2O_3 substrates. AlN/AlGaN strain-compensating layers and hybrid multiple-quantum-well structures were employed to improve the crystalline-quality of the InGaN active region. A bare LED showed that peak wavelength, light output power, and external quantum efficiency were 665 nm, 0.07 mW, and 0.19% at 20 mA, respectively. As its forward voltage was 2.45 V at 20 mA, the wall-plug efficiency was 0.14%. The characteristic temperature of the LEDs was 222 K at 100 mA evaluated from the temperature dependence of electroluminescence. © 2020 The Japan Society of Applied Physics

InGaN-based light-emitting diodes (LEDs) have been commercialized as highly efficient solid-state lighting sources. InGaN material is attractive for use in next-generation optoelectronic devices. It is possible to tune the emission wavelength in the fully visible spectral range using different In-content in $In_xGa_{1-x}N$. As a result, III-nitride semiconductors have an outstanding feature that they can produce the red, green, and blue LEDs for the realization of micro-LED displays and phosphor-free white LED lightings. The external quantum efficiency (EQE) of blue LEDs was exceeded by more than 80%.[1] However, the EQE is significantly lower in the green, yellow, and red spectral ranges.[2–13] The longer wavelength LEDs require higher In-content in InGaN as an active region. Several critical issues result from this high-In-content InGaN.

The first issue is low-temperature growth for high-In-content InGaN. The crystalline-quality of InGaN layers depends on growth temperature. This is because the lower temperature leads to many defects and rough surfaces by insufficient surface migration of adatoms.[14] The second issue is a tremendous strain in the InGaN layers since there is a significant lattice mismatch between InGaN and GaN. The strain induces misfit dislocations.[15,16] The third issue is the enhancement of the quantum-confined Stark effect (QCSE) in the high-In-content InGaN quantum wells (QWs).[17,18] The QCSE separates the electron and hole wavefunctions spatially in the QWs, which causes low internal quantum efficiency.

To achieve improved performance using the InGaN-based red LEDs, it is necessary to resolve these problems. In the previous reports, modification of the flow-channel could achieve an increase in the growth temperature of InGaN layers.[4,19] Also, the rapid growth rate increased growth temperatures.[20,21] High-temperature InGaN growth is a crucial technique to improve crystalline-quality of the high-In-content InGaN. Recently, longer wavelength InGaN-based LEDs have been developed using Al(Ga)N barrier layers.[6,10,22] This technique has significantly enhanced the EQE in the green-to-red spectral range. The Al(Ga)N layers are employed to improve the crystalline-quality of the whole InGaN active region by strain-compensating. Those Al(Ga)N layers also work to enhance the radiative recombination due to increase in the overlap of electron-hole wavefunctions by the higher potential barriers in conduction and valence bands.[10]

The Sn-doped ($\bar{2}01$) β-Ga_2O_3 is conductive and a good substrate for nitride growth.[23] In this work, we first demonstrated InGaN-based red LEDs on ($\bar{2}01$) β-Ga_2O_3 substrates. These LEDs achieved the lower forward voltage 2.45 V at 20 mA compared to the previous reports of InGaN-based red LEDs[6,8] and excellent temperature stabilities in the range of 660 nm.

The LED structures were grown by metalorganic vapor phase epitaxy (MOVPE) in a single-wafer horizontal reactor.[4,19] Figure 1 shows a cross-sectional schematic structure of a red LED. The LED structure adopted a hybrid multiple-quantum-well (MQWs) structure and a strain-compensating barrier structure for enhancing the light output power.[8,22] We used a 5 μm thick Si-doped n-GaN template grown on a Sn-doped ($\bar{2}01$) β-Ga_2O_3 substrate by MOVPE (by Tamura Co. and Novel Crystal Technology, Inc.).[23,24] SiN_x arrays were performed to improve light extraction efficiency and to be capable of the carrier conductivity between GaN and β-Ga_2O_3 substrate.[23,24] The geometry of SiN_x mask patterns is 2 μm diameter, 4 μm pitch, and 1 μm height. The full-width at half-maximums (FWHMs) of (0002) and ($10\bar{1}2$) planes X-ray rocking curve of the n-GaN layers were 280 arcsec and 276 arcsec, respectively. The growth of the LED structure on the n-GaN/($\bar{2}01$) β-Ga_2O_3 substrates is as follows: an n-side structure consists of an 1 μm thick Si-doped n-GaN layer; 15 periods uid-superlattices (SLs) structure with 6 nm thick GaN; and 2 nm thick $In_{0.08}Ga_{0.92}N$ layers. A 15 nm thick Si-doped n-GaN layer was grown on the SLs. In the active region, a hybrid MQWs structure consists of a 2 nm thick $In_{0.2}Ga_{0.8}N$ single quantum well (SQW) with 2 nm thick GaN, 18 nm thick $Al_{0.15}Ga_{0.85}N$ and 3 nm thick GaN barrier layers, and 2.5 nm thick $In_{0.35}Ga_{0.65}N$ double quantum wells (DQWs) as the active layers with 1.2 nm thick AlN, 2 nm thick GaN, 18 nm thick $Al_{0.15}Ga_{0.85}N$ and 3 nm thick GaN barrier layers. GaN replaced the $Al_{0.15}Ga_{0.85}N$ layer as an upper barrier layer of the second red QW. Then, a 15 nm thick uid-GaN layer was grown on DQW as the last barrier. The p-side layers consist of a 100 nm thick Mg-doped p-GaN layer and a 10 nm thick heavily Mg-doped p^+-GaN layer. The blue SQW contributes to improve the crystalline-quality of InGaN red

Content from this work may be used under the terms of the Creative Commons Attribution 4.0 license. Any further distribution of this work must maintain attribution to the author(s) and the title of the work, journal citation and DOI.

© 2020 The Japan Society of Applied Physics

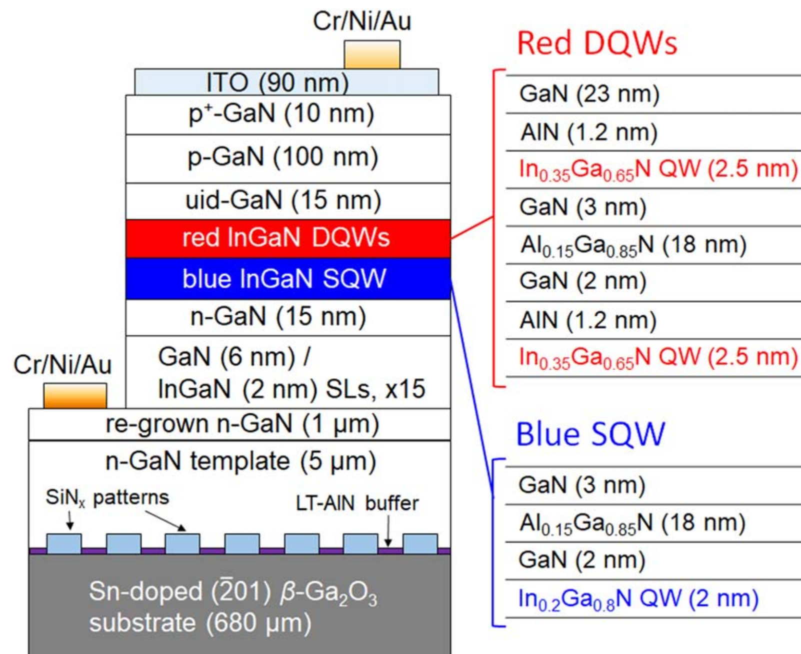

Fig. 1. (Color online) Cross-sectional schematic structure of the InGaN-based red LEDs.

QWs, which means to suppress the strain relaxation in the red QWs.[8] The InGaN red QWs were immediately capped by the AlN interlayers at the same growth temperature. The growth temperature ramped 155 °C higher than the InGaN red QWs for the growth of GaN/AlGaN/GaN barrier layers. This procedure significantly improved the crystalline-quality of the overall active region.[6,10,22] Those Al(Ga)N barrier structures provide the strain-compensating to suppress the generation of defects in the red DQWs.

The LED devices were fabricated in the standard face-up configuration. A 90 nm thick indium tin oxide layer was deposited on top of the p-layer as an ohmic contact by e-beam evaporation. The n-GaN layer was exposed by inductively coupled plasma etching to fabricate an n-contact electrode as a mesa-structure. We deposited a combination of Cr (50 nm)/Ni (20 nm)/Au (200 nm) metal structure as n- and p-pad contact electrodes. A bare LED chip configuration is $650 \times 250\,\mu m^2$ in size without resin molding. The LED devices were characterized by electroluminescence (EL) measurement under direct current (DC) operation at room temperature (RT). The output power of the bare LEDs was measured in a calibrated integrating sphere. The temperature dependence of EL was measured to characterize the quality of the LEDs. The LEDs were placed on a hot plate. The temperature of the hot plate was controlled in air ambient. The EL measurement was carried out when the temperature stabilized.

The EL spectra show the dependence of injection current at RT in Fig. 2. The LEDs show a large blueshift of the EL peak wavelength from 691 nm at 5 mA to 631 nm at 100 mA. The total blue-shifted amount is 60 nm in the range. The blueshift is a typical phenomenon in the c-plane InGaN QWs by the screening of the piezoelectric field and band filling of localized state.[17,18,25] The piezoelectric field in InGaN QWs depends on the In content. It also involved in the crystalline-quality of InGaN QWs, which released the strain in InGaN by the introduction of defects.[8] FWHMs were

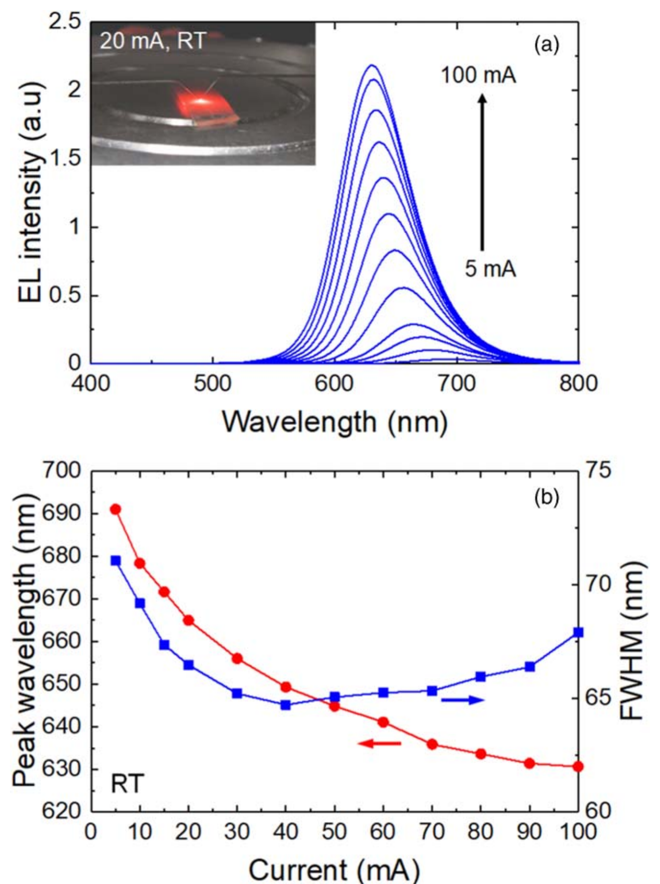

Fig. 2. (Color online) (a) EL spectra at various injection currents from 5 to 100 mA. The inset photograph shows the red LEDs driven at 20 mA. (b) EL peak wavelengths and FWHMs as functions of the injection current.

increased with the heat generation in the InGaN QWs at over 40 mA operation by the non-radiative recombination.[3]

The light output-current and forward voltage–current characteristics with various DC injection at RT are shown in Fig. 3. The light output and forward voltage for the LEDs

© 2020 The Japan Society of Applied Physics

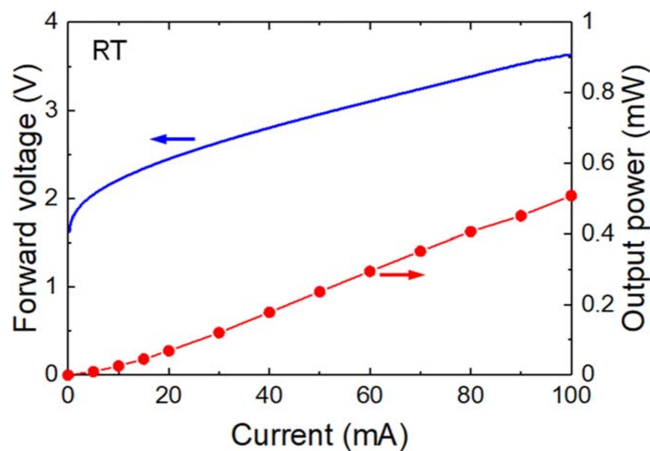

Fig. 3. (Color online) Light output-current and forward voltage–current characteristics of the red LEDs.

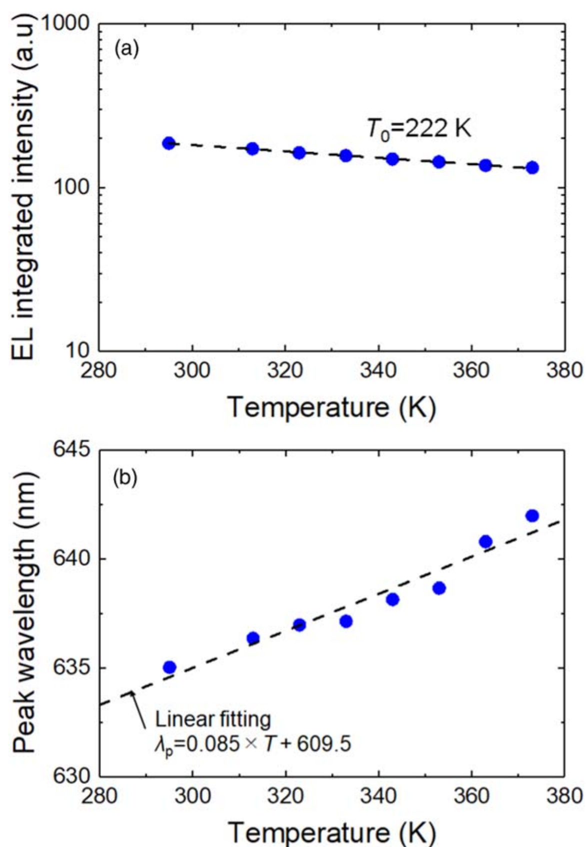

Fig. 4. (Color online) Temperature dependence of (a) EL integrated intensity and (b) peak wavelength from 22 °C to 100 °C.

were 0.07 mW and 2.45 V at 20 mA, respectively. In our LED configuration, β-Ga_2O_3 substrates probably do not contribute to low forward voltage operation because the injected current is parallelly passed through the n-GaN layers. Nevertheless, the forward voltage was significantly smaller compared with the previous report values (e.g. 3.7–4.4 V). We believe that the lower forward voltage was attributed to the hole injection via V-pits that generate from the InGaN SLs region.[12,26] The proper SLs structure is contributed to the high WPE of the LEDs. However, the forward voltage remains high compared to AlInGaP-based LEDs (e.g. 1.9 V at 20 mA)[27] because the AlN and AlGaN barriers work as significant potential barriers. The LEDs exhibited the EQE and WPE of 0.19% and 0.14% at 20 mA, respectively.

Figure 4(a) shows the temperature dependence of EL measurement at 100 mA. The EL integrated intensity markedly decreased with increasing stage temperature. The thermal droops of EL intensity can be explained by:

$$I = I_{T=295\mathrm{K}} \exp\left[-(T - 295)/T_0\right], \tag{1}$$

where I is the EL intensity, $I_{T=295\mathrm{K}}$ is the EL intensity at 295 K, T is the temperature of the sampling stage, and T_0 is the characteristic temperature.[28] We calculated T_0 by fitting formula (1) to the experiment results. We found that the T_0 values were 222 K at 100 mA. These values are lower than the 469.8 K reported for 630 nm AlInGaP-based LEDs at 100 mA in CW operation.[27] It has been reported that non-radiative recombination should become effectively at a higher temperature.[28–30] That means the InGaN-based red QWs dominate the non-radiative recombination process by QCSE and defects. Meanwhile, the EL peak wavelength was redshifted by increasing stage temperature, as shown in Fig. 4(b). This behavior is a typical phenomenon of semiconductor materials because the bandgap energy depends on temperature.[31] We found that the tendency of the EL peak-shift wavelength is 0.085 nm K^{-1}. In the case of 630 nm AlInGaP-based LEDs, it is shifted the tendency of 0.137 nm K^{-1}.[27] Therefore, InGaN-based LEDs are proper candidates for high-stability lightings by temperature.

In summary, we first demonstrated the InGaN-based LEDs on $(\bar{2}01)$ β-Ga_2O_3 substrates in the red spectral range. The light output, forward voltage, and EQE of the bare LEDs chips were 0.07 mW, 2.45 V, and 0.19% at 20 mA, respectively. The peak emission wavelength and FWHM were 665 nm and 67 nm at 20 mA, respectively. The LEDs showed temperature stability of the EL emission, which had the characteristic temperature of 222 K at 100 mA and the peak-shift wavelength of 0.085 nm K^{-1}.

Acknowledgments This work was financially supported by King Abdullah University of Science and Technology (KAUST) (BAS/1/1676-01-01).

ORCID iDs Daisuke Iida https://orcid.org/0000-0003-2896-754X Kazuhiro Ohkawa https://orcid.org/0000-0002-8728-3503

1) Y. Narukawa, M. Ichikawa, D. Sanga, M. Sano, and T. Mukai, J. Phys. D **43**, 354002 (2010).
2) S. Nakamura, M. Senoh, N. Iwasa, and S. Nagahama, Jpn. J. Appl. Phys. **34**, L797 (1995).
3) M. Funato, M. Ueda, Y. Kawakami, Y. Narukawa, T. Kosugi, M. Takahashi, and T. Mukai, Jpn. J. Appl. Phys. **45**, L659 (2006).
4) K. Ohkawa, T. Watanabe, M. Sakamoto, A. Hirako, and M. Deura, J. Cryst. Growth **343**, 13 (2012).
5) Y. Kawaguchi, C.-Y. Huang, Y.-R. Wu, Y. Zhao, S. P. DenBaars, and S. Nakamura, Jpn. J. Appl. Phys. **52**, 08JC08 (2013).
6) J. I. Hwang, R. Hashimoto, S. Saito, and S. Nunoue, Appl. Phys. Express **7**, 071003 (2014).
7) K. Kishino, A. Yanagihara, K. Ikeda, and K. Yamano, Electron. Lett. **51**, 852 (2015).
8) D. Iida, K. Niwa, S. Kamiyama, and K. Ohkawa, Appl. Phys. Express **9**, 111003 (2016).
9) A. Even, G. Laval, O. Ledoux, P. Ferret, D. Sotta, E. Guiot, F. Levy, I. C. Robin, and A. Dussaigne, Appl. Phys. Lett. **110**, 262103 (2017).
10) A. I. Alhassan, N. G. Young, R. M. Farrell, C. Pynn, F. Wu, A. Y. Alyamani, S. Nakamura, S. P. DenBaars, and J. S. Speck, Opt. Express **26**, 5591 (2018).
11) B. Mitchell, V. Dierolf, T. Gregorkiewicz, and Y. Fujiwara, J. Appl. Phys. **123**, 160901 (2018).
12) F. Jiang et al., Photonics Res. **7**, 144 (2019).

 © 2020 The Japan Society of Applied Physics

13) T. Ozaki, M. Funato, and Y. Kawakami, Appl. Phys. Express **12**, 011007 (2019).
14) R. A. Oliver, M. J. Kappers, G. A. D. Briggs, and C. J. Humphreys, J. Appl. Phys. **97**, 013707 (2005).
15) S. Srinivasan, L. Geng, R. Liu, F. A. Ponce, Y. Narukawa, and S. Tanaka, Appl. Phys. Lett. **83**, 5187 (2003).
16) D. Iida, Y. Kondo, M. Sowa, T. Sugiyama, M. Iwaya, T. Takeuchi, S. Kamiyama, and I. Akasaki, Phys. Status Solidi RRL **7**, 211 (2013).
17) T. Takeuchi, S. Sota, M. Katsuragawa, M. Komori, H. Takeuchi, H. Amano, and I. Akasaki, Jpn. J. Appl. Phys. **36**, L382 (1997).
18) T. Takeuchi, C. Wetzel, S. Yamaguchi, H. Sakai, H. Amano, I. Akasaki, Y. Kaneko, S. Nakagawa, Y. Yamaoka, and N. Yamada, Appl. Phys. Lett. **73**, 1691 (1998).
19) K. Ohkawa, F. Ichinohe, T. Watanabe, K. Nakamura, and D. Iida, J. Cryst. Growth **512**, 69 (2019).
20) S. Keller, B. P. Keller, D. Kapolnek, A. C. Abare, H. Masui, L. A. Coldren, U. K. Mishra, and S. P. Den Baars, Appl. Phys. Lett. **68**, 3147 (1996).
21) R. Hashimoto, J. I. Hwang, S. Saito, and S. Nunoue, Phys. Status Solidi C **10**, 1529 (2013).
22) D. Iida, S. Lu, S. Hirahara, K. Niwa, S. Kamiyama, and K. Ohkawa, J. Cryst. Growth **448**, 105 (2016).
23) M. M. Muhammed, N. Alwadai, S. Lopatin, A. Kuramata, and I. S. Roqan, ACS Appl. Mater. Interfaces **9**, 34057 (2017).
24) K. Iizuka, Y. Morishima, A. Kuramata, Y.-J. Shen, C.-Y. Tsai, Y.-Y. Su, G. Liu, T.-C. Hsu, and J. H. Yeh, Proc. SPIE **9363**, 93631Z (2015).
25) C. Li, Z. Ji, J. Li, M. Xu, H. Xiao, and X. Xu, Sci. Rep. **7**, 15301 (2017).
26) M. Liu, J. Zhao, S. Zhou, Y. Gao, J. Hu, X. Liu, and X. Ding, Nanomaterials **8**, 450 (2018).
27) H. K. Lee, D. H. Lee, Y. M. Song, Y. T. Lee, and J. S. Yu, Solid-State Electron. **56**, 79 (2011).
28) S. Chhajed, Y. Xi, Y.-L. Li, T. Gessmann, and E. F. Schubert, J. Appl. Phys. **97**, 054506 (2005).
29) S. Chhajed, J. Cho, E. F. Schubert, J. K. Kim, D. D. Koleske, and M. H. Crawford, Phys. Status Solidi A **208**, 947 (2011).
30) D. S. Meyaard, Q. Shan, J. H. Cho, E. F. Schubert, S. H. Han, M. H. Kim, C. S. Sone, S. J. Oh, and J. K. Kim, Appl. Phys. Lett. **100**, 081106 (2012).
31) Y. P. Varshni, Physica **34**, 149 (1967).

© 2020 The Japan Society of Applied Physics